Available online at www.sciencedirect.com

ScienceDirect

Geochimica et Cosmochimica Acta 173 (2016) 97–113

Geochimica et Cosmochimica Acta

www.elsevier.com/locate/gca

Oxygen isotope and petrological study of silicate inclusions in IIE iron meteorites and their relationship with H chondrites

Kathryn H. McDermott [a,b,*], Richard C. Greenwood [a], Edward R.D. Scott [c], Ian A. Franchi [a], Mahesh Anand [a,d]

[a] Planetary and Space Sciences, The Open University, Walton Hall, Milton Keynes MK7 6AA, United Kingdom
[b] School of Physical Sciences, Ingram Building, University of Kent, Canterbury CT2 7NH, United Kingdom
[c] Hawaii Institute of Geophysics and Planetology, University of Hawaii, Honolulu, HI 96822, USA
[d] Department of Earth Sciences, The Natural History Museum, London SW7 5BD, United Kingdom

Received 10 November 2014; accepted in revised form 14 October 2015; available online 28 October 2015

Abstract

The origin of silicate-bearing irons, especially those in groups IAB, IIICD, and IIE, is poorly understood as silicate should have separated rapidly from molten metal. Here we report the results of high precision oxygen isotope analysis of silicate inclusions in eleven group IIE meteorites and a petrological study of silicate inclusions in ten IIE irons including those in Garhi Yasin and Tarahumara, which have not been described in detail before. Oxygen isotopes have also been analysed in 20 H chondrites to investigate their possible relationship with the IIE irons.

Based on petrographic observations and mineral analysis, the silicate-bearing IIE meteorites have been divided into four types according to the nature of their silicate inclusions: (1) primitive chondritic, (2) evolved chondritic, (3) differentiated with >10 vol.% orthopyroxene, and (4) differentiated with <10 vol.% orthopyroxene. Each meteorite contains a single inclusion type. While inclusions in an individual IIE meteorite tend to show relatively limited $\Delta^{17}O$ variation, a wide range of values is seen in the dataset as a whole. Group IIE irons with differentiated silicates, with the exception of Colomera, have a range of mean $\Delta^{17}O$ values that is essentially identical to those of the H4-6 chondrites: 0.60–0.77‰ and 0.61–0.76‰, respectively. Colomera inclusions, which are differentiated with <10 vol.% orthopyroxene, have an anomalously high $\Delta^{17}O$ value and plot ~2σ away from the next nearest IIE iron. However, in view of the textural similarities to other IIE inclusions, a separate source for Colomera is deemed unlikely. Three IIE irons with primitive chondritic inclusions, Garhi Yasin, Netschaëvo, and Techado, have relatively low mean $\Delta^{17}O$ values of 0.56–0.57‰ as well as relatively reduced silicates with $Fa_{15–17}$ olivine, which have been called HH chondrites. Given the significant overlap in their oxygen isotope compositions, a genetic relationship between IIE irons and H chondrites is supported by our new data. However, derivation of both groups from one parent body seems unlikely. Instead, both groups probably sampled similar precursor materials and accreted at a similar nebular location.

Our data suggest that the IIE meteorites formed on an internally heated H/HH chondrite-like body that experienced the initial stages of differentiation in response to radiogenic heating. However, prior to full differentiation the IIE parent body experienced a major hit-and-run style collision that resulted in silicate-metal mixing. The initial stages of this event involved a phase of rapid cooling that prevented unmixing of metal and silicates. Reassembly of the IIE parent body produced a large regolith blanket that facilitated subsequent slow cooling. The IIE parent body has probably experienced numerous subsequent

* Corresponding author at: School of Physical Sciences, Ingram Building, University of Kent, Canterbury CT2 7NH, United Kingdom.
E-mail address: k.mcdermott@kent.ac.uk (K.H. McDermott).

http://dx.doi.org/10.1016/j.gca.2015.10.014

less catastrophic collisions. The development of alkali glass textures in some differentiated inclusions is probably the result of one of these later events.

1. INTRODUCTION

The formation and subsequent differentiation of small achondritic parent bodies took place early in Solar System history (Bizzarro et al., 2005; Kleine et al., 2005, 2009; Scherstein et al., 2006). Magmatic iron meteorites are generally accepted as representing material derived from the cores of these early-formed asteroids (Wasson and Richardson, 2001; Chabot and Haack, 2006; Goldstein et al., 2009). On the basis of Hf-W isotopic evidence, iron meteorites of the IIAB, IID, IIIAB, IVA and IVB groups are inferred to be samples from parent bodies that accreted less than 1 My after CAI formation (Kruijer et al., 2014).

In contrast to the magmatic iron meteorites, the genesis of silicate-bearing irons (IAB, IIICD, and IIE) is less well understood (Mittlefehldt et al., 1998; Wasson and Kallemeyn, 2002; Haack and McCoy, 2003; Goldstein et al., 2009; Tomkins et al., 2013; Ruzicka, 2014). In large part this relates to the fact that, due to the significant density contrast involved, segregation of metal and silicate should have taken place rapidly during partial melting. A wide range of complex models have been proposed to explain the origin of silicate-bearing irons. These generally invoke some combination of local to large-scale melting and impact-related mixing (Mittlefehldt et al., 1998; Wasson and Kallemeyn, 2002; Benedix et al., 2000, 2005; Ruzicka and Hutson, 2010; Ruzicka, 2014). Irons in group IIE are classified solely on the basis of the chemical composition of their metallic Fe–Ni as, unlike the more numerous IAB irons, they have remarkably diverse structures, mineralogy, and silicate inclusions (Buchwald, 1975; Scott and Wasson, 1976; Wasson and Wang, 1986).

Fourteen of the 21 presently recognised IIE irons contain silicate inclusions, which range from those with a chondritic composition, such as the large inclusion from Watson 001 (Watson) (Olsen et al., 1994), to more chemically fractionated types, such as those found in Kodaikanal (Burnett and Wasserburg, 1967a) and Colomera (Takeda et al., 2003). Fractionated inclusions, which are typically mm-to-cm in size and occupy ~5–10 vol.%, commonly take the form of feldspar-rich globules (Buchwald, 1975; Prinz et al., 1983; Ruzicka, 2014). Chondritic inclusions tend to be larger, angular and unevenly dispersed. In Watson, a single 11 cm long inclusion was identified (Olsen et al., 1994). Most inclusions contain Na-rich feldspar and orthopyroxene ± clinopyroxene and olivine, as well as various non-silicate phases, including Ca phosphates (apatite and merrillite), chromite and troilite.

Group IIE silicate inclusions have been divided into two types (Mittlefehldt et al., 1998): (i) chondritic, which have a chondritic or chondrite-like composition, and (ii) differentiated, which are more evolved. Three of the IIE irons with chondritic inclusions (Netschaëvo, Mont Dieu, and RBT 04186) contain relict or whole chondrules (Olsen and Jarosewich, 1971; Van Roosbroek et al., 2015; Meteoritical Bulletin Database). The composition of silicate inclusions in the chondritic group show strong similarities to that of the H chondrites (Olsen et al., 1994; Casanova et al., 1995; Van Roosbroek et al., 2015). This evidence, together with the presence of chondrules in some examples, has led to a widespread acceptance that the IIE inclusions are related to the H chondrites, or at least to some type of H chondrite-like material. However, in detail there remains considerable controversy about the exact nature of the H chondrite-IIE relationship. While a direct link between the H chondrite parent body and the IIEs is favoured by some (e.g. Gaffey and Gilbert, 1998), others have argued against their derivation from a common source (Bogard et al., 2000). Bild and Wasson (1977) suggest that the IIE silicates formed from ordinary chondrite-like material that is more FeO-poor and metal-rich than the H chondrites—so-called HH chondrites (Russell et al., 1998; Troiano et al., 2011). There is also no agreement about the mechanism by which the IIE silicate inclusions were incorporated into their host metal. While some form of impact mixing is favoured by most (e.g. Wasson and Wang, 1986; Olsen et al., 1994; Casanova et al., 1995; Ruzicka and Hutson, 2010; Van Roosbroek et al., 2015), more deep-seated formation within a single parent body has also been proposed (Wasserburg et al., 1968; McCoy, 1995). Wasserburg et al. (1968) summarised their model in terms of "plums of iron in a pudding of silicate".

Oxygen isotopic analyses of both IIE silicate inclusions and H chondrites obtained by the externally-heated Ni bomb technique (Clayton and Mayeda, 1963) showed significant overlap, with a mean $\Delta^{17}O$ value for the equilibrated H chondrites of $0.73 \pm 0.09‰$ (1σ) compared to $0.59 \pm 0.07‰$ (1σ) for the IIE silicate inclusions (Clayton et al., 1991; Clayton and Mayeda, 1996). This overlap led Clayton and Mayeda (1996) to suggest that the two were not merely related by impact mixing alone, but instead there existed: "a genetic, rather than accidental association between H chondrites and IIE irons." However, Franchi (2008) cast doubt on a close relationship between the H chondrites and IIE silicate inclusions. He cited the more reduced state of the chondritic silicates in IIE irons and the evidence from high precision laser fluorination analyses of nine equilibrated H chondrites by Folco et al. (2004) that yielded a higher mean $\Delta^{17}O$ value of $0.77 \pm 0.04‰$ (1σ), "essentially distinct from the IIE irons". Franchi (2008) suggested that this evidence raised the possibility that the IIEs formed on a parent body distinct from that of the H chondrites.

In order to understand the origin of the IIE meteorites we have undertaken a detailed oxygen isotope study of their silicate inclusions by laser fluorination. We have also

analyzed a suite of 20 H chondrites, which includes all of the samples previously studied by Folco et al. (2004), to clarify the possible relationship between IIE irons and H chondrites. In addition to oxygen isotope analyses, we have also studied the petrography and mineral chemistry of selected inclusions with the aim of investigating the origin of the IIE meteorites and the nature of their parent body, or bodies.

2. SAMPLES AND METHODS

2.1. Sample preparation

Details of the samples used in this study are given in Table 1. Bulk samples for oxygen isotope analysis were, in general, extracted from cut slabs and blocks using stainless steel tools. Mineral separates for Colomera, Kodaikanal, Miles, and Weekeroo Station were kindly provided by Robert Clayton. For the original source of these samples and the separation techniques employed, see Clayton and Mayeda (1996) and references therein.

To ensure a representative bulk sample from each inclusion a minimum of 10 mg of material was extracted and crushed in an agate pestle and mortar. Aliquots of approximately 2 mg were then taken from these homogenized powders for oxygen isotopic analysis. All metal was removed by hand. The H chondrites analysed for this study were taken from larger powdered and homogenized aliquots, prepared from interior chips of generally >100 mg. Some IIE samples were provided as bulk powders (TYR 05181, Tarahumara, Miles, Netschaëvo, and Miles), or as powdered mineral separates of feldspar or glass (Table 1) and so only oxygen isotopic analysis could be undertaken on these materials.

2.2. Mineral analysis

Major and minor element analysis of mineral phases in IIE silicate inclusions was undertaken using an FEI Quanta 200 FIB scanning electron microscope (SEM) and a Cameca SX-100 electron microprobe at the Open University. Both systems were used to acquire quantitative major element analysis, element maps and back-scattered electron images of the IIE silicate samples. Where a sample could be mounted in a 1 inch resin block, or a polished thin section could be prepared, analyses were undertaken by electron microprobe analysis (EMPA), whereas samples that could not be mounted were analysed using the SEM. For the EMPA analysis an accelerating voltage of 20 kV, a spot size of 10 μm and a beam current of 20 nA were generally used for quantitative analysis, whereas for the SEM work an accelerating voltage of 20 kV, a spot size of 4.5 μm and a beam current of 0.6 nA were normally employed.

Using the computer program QUILF (Lindsley and Andersen, 1983; Andersen et al., 1993), closure temperature estimates have been obtained for coexisting orthopyroxene and clinopyroxene compositions in differentiated IIE silicates.

2.3. Oxygen isotope analysis

Oxygen isotope analysis was carried out at the Open University using an infrared laser-assisted fluorination system (Miller et al., 1999). Silicates were heated in the presence of BrF_5 to liberate oxygen, which was purified by passing it through a clean-up system, consisting of two liquid nitrogen traps separated by a heated KBr tube. The oxygen isotope composition of the purified gas was analysed using a MAT 253 isotope ratio mass spectrometer. Internal (obsidian) and external (UWG-2 Garnet (Valley et al., 1995)) standards were run at the start of each analytical session. An estimate of the present level of precision of the Open University system is provided by 39 analyses of our internal obsidian standard undertaken during six separate sessions in 2013, which gave the following combined results: ±0.05‰ for $\delta^{17}O$; ±0.09‰ for $\delta^{18}O$; ±0.02‰ for $\Delta^{17}O$ (2σ). The precision (2σ) quoted for individual meteorite samples is based on replicate analyses.

Oxygen isotopic analyses are reported in standard δ notation, where $\delta^{18}O$ has been calculated as: $\delta^{18}O = [(^{18}O/^{16}O)_{sample}/(^{18}O/^{16}O)_{ref} - 1] \times 1000(‰)$ and similarly for $\delta^{17}O$ using the $^{17}O/^{16}O$ ratio, the reference being VSMOW: Vienna Standard Mean Ocean Water. $\Delta^{17}O$, which represents the deviation from the terrestrial fractionation line, has been calculated using the linearized format of Miller (2002):

$$\Delta^{17}O = 1000\ln(1 + \delta^{17}O/1000) - \lambda 1000\ln(1 + \delta^{18}O/1000)$$

where $\lambda = 0.5247$, which was determined using 47 terrestrial whole-rock and mineral separate samples (Miller et al., 1999; Miller, 2002). In Tables 6 and 7, the "conventional" ($\Delta^{17}O = \delta^{17}O\text{-}0.52\ \delta^{18}O$) and "linearized" versions of $\Delta^{17}O$ are both given for comparison. However, only "linearized" $\Delta^{17}O$ values are plotted and discussed in the text.

3. PETROLOGY AND GEOTHERMOMETRY

3.1. Classification scheme

We examined in detail the petrology of 10 out of the 14 known silicate-bearing iron meteorites (Table 1). Based on our results and those of previous studies (Wasserburg et al., 1968; Bence and Burnett, 1969; Bunch et al., 1970; Olsen and Jarosewich, 1971; Bild and Wasson, 1977; Osadchii et al., 1982; Prinz et al., 1983; Olsen et al., 1994; Casanova et al., 1995; Ikeda et al., 1997; Bogard et al., 2000; Takeda et al., 2003; Ruzicka and Hutson, 2010), the silicate-bearing IIE iron meteorites have been classified on the basis of their texture and composition into two major types (chondritic and differentiated), each of which is further divided into two subtypes. The criteria used to define each subtype are summarized in Table 2 and the textures shown in Fig. 1. This classification scheme is an extension of that proposed by Mittlefehldt et al. (1998).

The scheme is designed to separate those IIEs which have silicate inclusions showing features consistent with extensive fractionation (high and low Opx subtypes), from those which have primitive compositions similar to

Table 1
Group IIE iron meteorites, their silicate inclusions, and meteorite samples used for petrological and oxygen isotopic analysis and their sources.

Meteorite name	Year found	Silicate incl.	References	Class*	Petrological analysis	Section source†	O isotopic analysis	Sample source†
Arlington	1894	Not found	15	IIE-An	—		—	
Barranca Blanca	1855	Not found	15	IIE-An	—		—	
Colomera	1912	Differentiated	0, 1, 4	IIE	EMPA	JD (4578-2)	Diopside and Feldspar	Clayton
Elephant Mor. 83390	1983	Not found	2	IIE-An	—		—	
Elga	1959	Differentiated	1, 5	IIE	EMPA	JD (4874-1)	—	
Garhi Yasin	1917‡	Chondritic	1	IIE	SEM	NHM (BM1924832)	Bulk	NHM (BM1924832)
Kodaikanal	1898	Differentiated	0, 1, 6	IIE	EMPA	JD (4629-1), NHM (BM 1920310)	Glass, augite, alkali glass	Clayton
Leshan	1964	Not found	2	IIE	—		—	
Miles	1992	Differentiated	1, 7, 8, 9	IIE	EMPA	JD (4866-3), NHM (BM1995M1)	Bulk and feldspar	Clayton, USNM
Mont Dieu	1994	Chondritic	3	IIE	—		—	
Netschaëvo	1846	Chondritic	0, 1, 12, 13	IIE-An	SEM and EMPA	USNM (494-2) JD (195-1), NHM(3393)	Bulk	AMNH, USNM
NWA 5608	2007	Differentiated	16	IIE	—		Bulk	JW
NWA 6716	2010	Not found	2	IIE	—		—	
Roberts Massif 04186	2004	Chondritic	2	IIE	—		—	
Tarahumara	1994	Differentiated	1, 16	IIE	SEM and EMPA	USNM (7194), RH	Bulk	USNM 7194
Taylor Glacier 05181	2005	Differentiated	2	IIE	—		Bulk	NASA-JSC
Techado	1983	Chondritic	1, 10	IIE	EMPA	AB	Bulk	AB
Tobychan	1971	Not found	17	IIE	—		—	
Verkhne Dnieprovsk	1876	Not found	18	IIE	—		—	
Watson 001	1972	Melted chondritic	1, 11	IIE	SEM and EMPA	JD (4762-1), NHM (BM1993M16), AE USNM (6829, 6489-2)	Bulk	AMNH, AE
Weekeroo Station	1924	Differentiated	0, 1, 14,	IIE-An	SEM and EMPA	JD (2620-5), USNM, AMNH,	Bulk and feldspar	Clayton, NHM (BM 1929196)

References: 0 – Bunch et al. (1970); 1 – this work; 2 – Meteoritical Bulletin Database (see http://www.lpi.usra.edu/meteor/metbull.php); 3 – Van Roosbroek et al. (2015); 4 – Takeda et al. (2003); 5 – Osadchii et al. (1982); 6 – Bence and Burnett (1969); 7 – Ebihara et al. (1997); 8 – Ikeda et al. (1997); 9 – Ruzicka and Hutson (2010); 10 – Casanova et al. (1995); 11 – Olsen et al. (1994); 12 – Bild and Wasson (1977); 13 – Olsen and Jarosewich (1971); 14 – Ruzicka et al. (1999); 15 – Buchwald (1975); 16 – Ruzicka (2014); 17 – Wasson and Wang (1986); 18 – Buchwald and Clarke (1987).

* Classification as IIE or IIE-An is from Wasson and Wang (1986) and Meteoritical Bulletin Data Base. Most IIE-An irons were labelled on the basis what appeared to be an anomalous feature when only twelve IIE and IIE-An irons were known. Yamato 791093 was excluded as it is a small H6 chondrite that was enriched in metal and troilite by shock melting (Ikeda et al., 1997), like several other small meteorites (Schrader et al., 2010). Kavapura was excluded as Ray et al. (2014) found that it was an IVA iron, not a IIE member.

† Source abbreviations: JD – J. Delaney, USNM – US National Museum of Natural History (Smithsonian Inst.), NHM – Natural History Museum, London, JW – J. Wasson, RH – R. Haag, AMNH – American Museum of Natural History, New York, AE – A. Ehlmann, Texas Christian University; JSC – NASA Johnson Space Center, Houston, AB – A. Brearley, University of New Mexico.

‡ One fall; rest are finds.

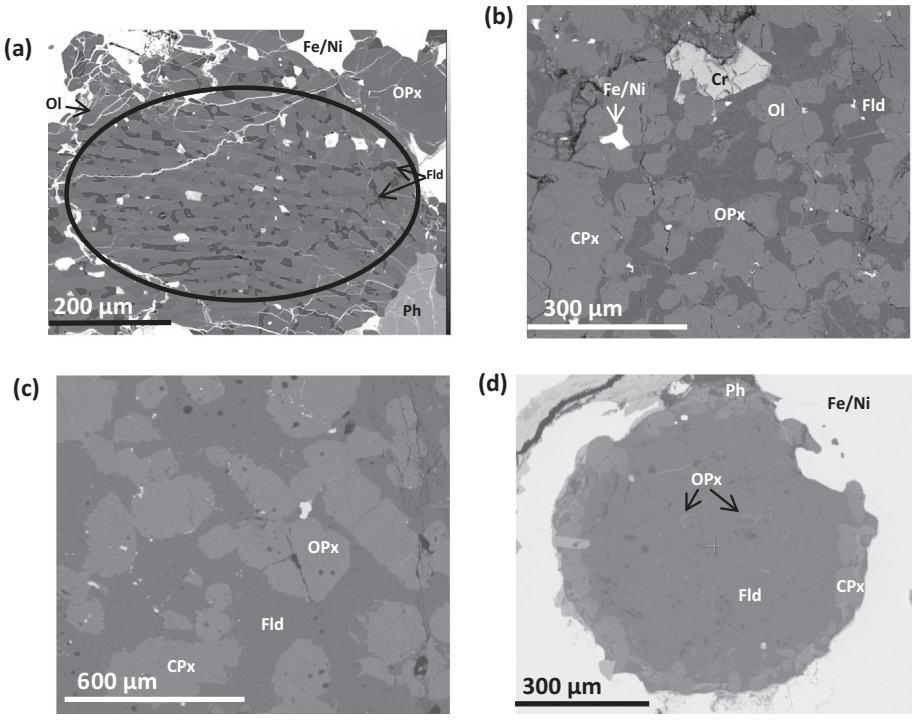

Fig. 1. Back-scattered electron images of silicate inclusions in four IIE iron meteorites illustrating textural features described in Section 3. Key: Ol = Olivine, OPx = Orthopyroxene, Fld = Feldspar, CPx = Clinopyroxene, Ph = Phosphate, Cr = Chromite, Fe/Ni = Fe, Ni metal. (a) Primitive chondritic inclusion in Techado showing olivine, pyroxene, small plagioclase grains, large metallic blebs, and a barred chondrule-like texture. (b) Evolved chondritic inclusion in Watson showing clinopyroxene along with olivine, orthopyroxene, and albitic feldspar, and very rare metallic blebs. (c) High Opx – differentiated inclusion in Weekeroo Station showing the feldspar matrix and angular phenocrysts of clinopyroxene and orthopyroxene with exsolution striations. (d) Low Opx – differentiated inclusion in Colomera showing the dominant feldspar matrix, which contains small rounded inclusions of orthopyroxene. The inclusion is rimmed by euhedral phenocrysts of clinopyroxene and Ca – phosphate minerals.

chondrites and show few melted or differentiated textural features (primitive and evolved chondritic subtypes). The subtypes outline in Table 2 also display variable metal contents within inclusions. Thus, the primitive chondritic inclusions often contain >10 vol% FeNi metal and this decreases to <1 vol% in the low Opx-differentiated subtype (Tables 2 and 3). The variation in composition, mineralogy and texture from the primitive chondritic subtype through to the low Opx-differentiated subtype (Table 2) appears to reflect increasing degrees of differentiation. Although the mineralogy and texture vary from subtype to subtype, mineral compositions and modal abundances are uniform within individual IIE meteorites, with little variation observed in members of a single subtype.

3.2. Primitive chondritic subtype

Three IIE irons that we studied contain silicate inclusions with chondritic textures and mineralogy: Netschaëvo, Techado, and Garhi Yasin. Chondrules were reported in Netschaëvo by Olsen and Jarosewich (1971) and Bild and Wasson (1977) but they were not observed in Techado by Casanova et al. (1995). However, we observed a stretched and rounded, barred feature in Techado, which we interpret to be a chondrule (Fig. 1a). Mont Dieu also contains silicate inclusions that contain chondrules (Van Roosbroek et al., 2015).

Mineral compositions in the chondrules are indistinguishable from that elsewhere in the inclusions indicating that these chondrules were equilibrated and are not exotic features. The mineralogy of the primitive chondritic inclusions is dominated by olivine and orthopyroxene, with interstitial Na-rich feldspar and some grains of Ca phosphate (Table 3). Rounded blebs of FeNi metal and schreibersite commonly make up >10 vol% of the inclusions (Fig. 1a).

Mean olivine compositions in Netschaëvo, $Fa_{15.0}$, and Techado, $Fa_{16.3}$, are similar. Olivine in the chondrules and matrix of the Mont Dieu inclusions is also homogeneous with $Fa_{15.7}$ (Van Roosbroek et al., 2015). Orthopyroxene has a compositional range of $Fs_{12.8–16.5}En_{81.9–86.2}Wo_{<5.3}$ with the average for each sample being: Netschaëvo: $Fs_{13.9}En_{85.0}Wo_{1.1}$, Techado: $Fs_{15.1}En_{83.3}Wo_{1.6}$, and Mont Dieu: $Fs_{14.4}$ (Van Roosbroek et al., 2015). The feldspar in these silicate inclusions is interstitial to the mafic minerals and metal. The feldspar-rich regions ($Ab_{80.0–81.6}An_{13.2–15.3}Or_{4.7–5.3}$) are elongated, up to 200 µm long and are compositionally uniform throughout the sample, with no evidence of alteration or antiperthitic textures.

Silicates in Garhi Yasin were described by Buchwald (1975) but not analysed by him. The inclusion we studied displays similar textures, mineralogy and composition to that in Techado, however, distinct chondrule-like features, were not observed. Olivine ($Fa_{16.8}$) and orthopyroxene

Table 2
Classification of the silicate-bearing IIE members showing the criteria for the two main groups and sub groups of silicate inclusions.

Type	Criteria	Subtype	Criteria	IIE irons
Chondritic	Chondritic bulk composition.	Primitive Chondritic	High metal content >5 vol.%	Netschaevo Mont Dieu
	Olivine present.		Chondrules generally present	Garhi Yasin Techado
	Moderate to high metal content >2 vol.%		Clinopyroxene phenocrysts	
		Evolved chondritic	Chondrules absent Moderate metal content 2–5 vol.%	Watson
Differentiated	Non-chondritic bulk composition.	High OPx-differentiated	>10 vol.% Opx	Weekeroo Station Miles
	Olivine absent Low metal content <2 vol.%		Low metal content 1–2 vol.%	Tarahumara
		Low OPx-differentiated	<10 vol.% Opx	Kodiakanal Colomera
			Very low metal content <1 vol. %	Elga

($Fs_{14.6}En_{83.6}Wo_{1.8}$) are the dominant minerals (Table 3) and form rounded grains between 50 and 300 μm in maximum diameter. The olivine grains exhibit a high degree of homogeneity and often occur within and adjacent to the larger orthopyroxene grains. Feldspar ($Ab_{82.6}An_{12.1}Or_{5.3}$) is interstitial to orthopyroxene and olivine. In a few areas, K-rich feldspar is present as needle-like striations within the albitic plagioclase, indicative of an antiperthitic texture up to 50 μm in length and <10 μm wide.

3.3. Evolved chondritic

Watson is currently the only identified member of the evolved chondritic subtype and the only IIE to contain a single large silicate inclusion (7 cm by 11 cm) (Olsen et al., 1994). It has a chondritic composition, but is distinct from primitive chondritic inclusions as it contains clinopyroxene phenocrysts, a melted texture (Olsen et al., 1994), and a lower volume of metal (Fig. 1b). Olivine ($Fa_{19.9}$) and orthopyroxene ($Fs_{16.9}En_{79.5}Wo_{3.6}$) in Watson are homogeneous. Feldspar is interstitial and has a composition ($Ab_{85.7}An_{3.8}Or_{10.4}$), similar to that in primitive chondritic samples. It shows antiperthitic textures, similar to those observed in Garhi Yasin. Minor clinopyroxene ($Fs_{8.8}En_{51.3}Wo_{39.9}$) forms homogeneous anhedral crystals between 200 and 400 μm in size. The non-silicate component in the inclusion includes minor troilite, chromite, and merrillite.

3.4. High Opx-differentiated subtype

Inclusions within the high Opx-differentiated subtype have non-chondritic compositions and mineralogy dominated by feldspar and clinopyroxene, with olivine being either minor or absent. Orthopyroxene ($Fs_{76.4}$ $En_{20.8}Wo_{2.8}$) is a common phase, >10 vol.%, and often displays exsolution features (Fig. 1c). Na-rich feldspar is homogeneous and appears to be the only phase present in some inclusions. However, this may be a sampling artefact. Minor phases in these inclusions include chromite, Ca phosphates (merrillite and whitlockite) and troilite. FeNi metal is found only in small (~100 μm) areas of mesostasis in the feldspar-dominated areas of Weekeroo Station.

Inclusions in Weekeroo Station show many similarities to the other members of this subtype, Miles and Tarahumara, including exsolution features and antiperthitic textures but are more Fe-rich (Table 4). Fe enrichment is observed in orthopyroxene and to a lesser extent clinopyroxene. Ruzicka et al. (1999) found that orthopyroxene in Weekeroo Station shows a large variation in Fe/Mg. Feldspar in Weekeroo Station shows greater affinities with the chondritic IIEs than other members of this subtype.

3.5. Low Opx-differentiated

These inclusions are dominated by feldspar and clinopyroxene; orthopyroxene is less abundant than in the high Opx subtype, a feature which provides the main criterion for separating them (Fig. 1d). Olivine is absent from these inclusions and Fe/Ni material is <1 vol%. This subtype has three members: Kodaikanal, Colomera and Elga (Table 2). Kodaikanal and Colomera contain feldspar-rich inclusions with little to no gabbroic texture present and orthopyroxene as minor, elongated crystals (250 μm long). Elga is distinct, with a much more porphyritic texture of prismatic clinopyroxene ($Fs_{10.0}En_{45.8}Wo_{44.2}$) grains within a Na-feldspar matrix. Most inclusions observed in the sample of Elga studied in this project were dominated by prismatic unzoned clinopyroxene crystals up to 500 μm in length, with basal sections up to 100 μm. Clinopyroxene forms radiating bundles within the K–Na-rich glass and shows evidence of twinning. Large, rare, zoned Ca–phosphates are also found in these K-rich glass bearing inclusions. Other inclusions observed in Elga, that are located within a Na-rich glass ($SiO_2 = 71.5$ wt%) rather than a crystalline Na–K feldspar, have similar clinopyroxene compositions. Orthopyroxene

Table 3
Modal mineral abundances (vol.%) in group IIE inclusions from previous authors* and this study.†

Mineral	Primitive chondritic			Evolved chondritic	High Opx-differentiated			Low OPx-differentiated		
	Netschaëvo	Techado	Garhi Yasin†	Watson	Miles	Weekeroo St	Tarahumara†	Elga†	Colomera	Kodaikanal†
Olivine	26	40.	51	57	–	–	–	–	–	–
Orthopyroxene	52	40	35	23	23	24	13	–	3.0	8.0
Clinopyroxene	5.0	0.0	0.0	5.0	33	16	12	25	28	–
Plag-Trid-Glass	14	19	13	12	43	59	70	64	67	88
Ca–phosphate	2.0	1.0	0.9	1.0	0.3	1.0	4.4	10	1.0	4.0
Total	99	100	99.9	98	99.3	100	99.4	99	99	100
Metal	>10	>10	5–10	2–5	1–2	1–2	1–2	<1	<1	<1

This signifies the analyses that have been completed in this study alone.
* Netschaevo (Olsen and Jarosewich, 1971); Techado and Miles (Bogard et al., 2000); Weekeroo Station, Colomera and Watson (Prinz et al., 1983).

was not observed in our Elga sample, but some analyses are reported by Osadchii et al. (1982).

Orthopyroxene ($Fs_{18.2}En_{80.2}Wo_{1.6}$) in Kodaikanal forms small elongated grains up to 250 μm in length along with rare large merrillite, as reported by Bence and Burnett (1969). The composition of the inclusions we studied appear to be uniform, with most of the feldspar being sanidine with no observed antiperthitic texture. Clinopyroxene was not observed in our sample, but has been reported by Bence and Burnett (1969), who stated that the high temperature form of the sodic feldspar suggested that the silicate cooled rapidly from a high temperature.

Silicate inclusions in Colomera show similarities to those in Kodaikanal and have a high modal abundance (60%) of feldspar, which is homogeneous. Sanidine was not observed in the sample of Colomera analysed for this study, though it has been previously reported in a large surface inclusion (Wasserburg et al., 1968; Takeda et al., 2003).

Small volumes of glass have also been observed in these samples and in the mesostasis areas of the High Opx-differentiated subgroup. The glass is extremely siliceous and rich in alkalis. Ruzicka (2014) suggests that this Si-rich glass could have been formed by rapid immiscible separation of a Si-rich liquid, or it could be a shock feature and provide no evidence about the cooling rates of the primary minerals.

3.6. Two-pyroxene geothermometry

The results of two-pyroxene geothermometry calculations using the program QUILF (Andersen et al., 1993) are given in Table 5. This method provides an estimate of pyroxene closure temperatures which in turn can be interpreted in terms of cooling rates. Thus, those samples that record the lowest closure temperatures would have cooled more slowly than those that give higher temperatures, all other factors being equal. The technique requires that both orthopyroxene and clinopyroxene are present in a sample and as a consequence closure temperatures for the primitive chondritic inclusions cannot be calculated. The results of pyroxene thermometry calculations indicate that Colomera, the most differentiated IIE sample analysed in this study, records the lowest closure temperature of 860 ± 99 °C. This suggests that it experienced the slowest cooling rate of any IIE for which pyroxene thermometry data are available. The IIE members, Weekeroo Station, Miles and Tarahumara all have closure temperatures of around 1020 °C, with the exact calculated temperatures being 1017 ± 76 °C, 1029 ± 22 °C and 1028 ± 17 °C respectively. The evolved chondritic sample Watson has a closure temperature of 1100 ± 36 °C, indicating that it experienced faster cooling than the differentiated samples of Weekeroo Station, Miles and Tarahumara, which in turn cooled more rapidly than the low OPX-differentiated IIE sample Colomera. These results suggest that a general correlation exists between the cooling rate (closure temperature) experienced by an IIE member and the degree of differentiated experienced by its silicate material, based on textural and mineralogical evidence. Preservation of equilibration temperatures in the range of 800–1100 °C suggests relatively rapid cooling below the

Table 4
Bulk chemistry of silicate inclusions in IIE meteorites calculated using the modal abundances in Table 3 and average mineral compositions (see Appendix).

	Bulk chemistry											Ol		OPX			CPX			Plag		
IIE Sample	P_2O_5	SiO_2	TiO_2	Al_2O_3	Cr_2O_3	MgO	CaO	MnO	FeO	NiO	Na_2O	K_2O	Total	Fa	Fo	Fs	En	Wo	Fs	En	Wo	Ab	An	Or
Netschaëvo	1.0	51.7	0.1	3.3	0.1	30.5	1.7	0.4	9.2	0.0	1.3	0.1	99.5	15.0	85.0	13.9	85.0	1.1	–	–	–	80.0	15.3	4.7
Techado	0.5	50.1	0.1	4.4	0.1	30.5	1.3	0.4	10.5	0.0	1.9	0.2	100.0	16.3	83.7	15.1	83.3	1.6	–	–	–	81.6	13.1	5.3
Garhi Yasin	0.0	48.7	0.1	3.0	0.1	33.6	0.7	0.4	11.6	0.0	1.3	0.1	99.6	16.8	83.2	14.6	83.6	1.8	–	–	–	82.6	12.1	5.3
Watson	0.2	46.4	0.1	2.6	0.2	31.6	1.9	0.4	13.5	0.0	1.3	0.2	98.4	19.9	80.1	16.9	79.5	3.6	8.8	51.3	39.9	85.7	3.9	10.4
Miles	0.2	59.0	0.3	9.0	0.6	12.0	7.1	0.3	5.4	0.1	4.5	0.3	98.8	–	–	20.8	76.4	2.8	10.6	50.0	39.4	89.8	6.2	4.0
Weekeroo St	0.5	61.2	0.3	11.9	0.2	7.5	5.4	0.5	7.3	0.0	5.2	0.6	100.6	–	–	35.8	60.2	4.0	16.1	44.5	39.4	80.7	13.5	5.8
Tarahumara	1.9	63.1	0.2	14.4	0.2	5.3	4.3	0.1	2.5	0.0	5.4	3.5	101.0	–	–	21.1	75.9	3.0	10.9	47.1	42.0	68.1	2.6	29.3
Elga	4.4	58.6	0.5	10.9	0.4	4.3	9.0	0.1	1.8	0.0	3.8	4.4	98.2	–	–	–	–	–	9.8	47.1	43.1	54.3	0.1	45.6
Colomera	0.5	62.3	0.4	13.5	0.6	5.1	6.4	0.1	2.3	0.0	7.2	0.9	99.3	–	–	18.4	80.4	1.2	11.2	45.2	43.6	89.5	2.4	8.1
Kodaikanal	2.2	64.9	0.5	15.1	0.0	2.7	2.1	0.0	1.4	0.0	4.1	6.8	99.9	–	–	18.2	80.2	1.6	–	–	–	46.5	0.4	53.1

equilibration temperatures. Ruzicka (2014) infers from the presence of glass in differentiated inclusions that they cooled through this temperature range at >2.5 °C/h.

4. OXYGEN ISOTOPE ANALYSIS

4.1. IIE silicates

The results of high precision oxygen isotope analysis of IIE silicate inclusions, for both whole rocks and mineral separates, are given in Table 6 and plotted in Figs. 2 and 3. Feldspars separated from Colomera, Weekeroo Station and Miles show heavier $\delta^{17}O$ and $\delta^{18}O$ values than the associated diopside or whole rock analyses, a feature which reflects normal equilibrium fractionation (Onuma et al., 1972). However, all phases analysed from an individual meteorite have similar $\Delta^{17}O$ values and therefore define a common mass fractionation line (Fig. 2). The complete dataset for the IIEs shows a significant range in $\Delta^{17}O$ values (0.32‰) (Fig. 2, Table 6), with a mean of 0.68 ± 0.20‰ (2σ).

The primitive chondritic inclusions show limited $\Delta^{17}O$ variation and display the lowest $\Delta^{17}O$ values seen in any of the IIE silicates. Netschaëvo has a very low $\delta^{18}O$ value of 3.06‰, whereas Techado and Garhi Yasin have $\delta^{18}O$ values within the range of the differentiated IIEs (4.74‰ and 4.48‰, respectively). The differentiated IIE irons, both low and high Opx subtypes, show a wide range of $\Delta^{17}O$ values, from 0.60‰ to 0.88‰ (Fig. 2), which, with the possible exception of Colomera, appear to form a continuum with the primitive chondritic inclusions. In terms of its $\Delta^{17}O$ composition, Colomera plots $\sim 2\sigma$ away from the closest other IIE sample and therefore can be considered an outlier from the main IIE group. This could be interpreted as indicating that Colomera represents material derived from a different parent body to the other IIEs. However, it is unclear why Colomera should have such an elevated $\Delta^{17}O$ composition. In terms of texture, mineralogy and geochemistry, its inclusions are similar to other members of the low Opx subtype, such as Kodaikanal.

One of the differentiated samples, TYR 05181, plots close to members of the primitive chondritic subtype (Fig. 2). It is likely that its oxygen isotope composition has been disturbed due to terrestrial weathering, which would result in its primary values being shifted towards the terrestrial fractional line (TFL, $\Delta^{17}O = 0$). However, the sample was provided as a powder and the extent of terrestrial weathering of this sample has not been evaluated as part of this study. Silicate material in this meteorite was studied by T. McCoy (see Meteoritical Bulletin Database) and described as being similar to that in Miles.

4.2. H3-6 chondrites

High precision oxygen isotope analysis was undertaken on 19 equilibrated H4-6 chondrites and 1 unequilibrated H3 chondrite (Dhajala) (Table 7, Fig. 2). These data allow a direct comparison between the oxygen isotope fields of the IIEs and H chondrites based on data that were acquired using the same analysis method and instrumentation. The

H chondrite data define a field with a $\Delta^{17}O$ range of 0.15‰ and a mean value of 0.70 ± 0.08‰ (2σ) (Table 7, Fig. 2). The H chondrites also show a significant variation with respect to $\delta^{18}O$ (3.83–4.67‰), with a mean value of 4.17 ± 0.42‰ (2σ).

Following a review by John Wasson of an earlier version of this paper, we reanalysed all nine H4-6 chondrites that were analysed by Folco et al. (2004). We thank him for pointing out a discrepancy in the H chondrite oxygen isotope data with our study. A comparison between our new data and those of Folco et al. (2004) reveals a consistent difference in $\delta^{18}O$ values between the two datasets. The Folco et al. (2004) data are on average displaced by 0.43‰ towards lighter values compared to the same nine samples analysed in this study (Table 7, Fig. 3). In terms of $\Delta^{17}O$ values, the Folco et al. (2004) samples are on average displaced to higher values by 0.04‰ compared to the same samples run in this study. The Folco et al. (2004) data were collected at the Open University using an older generation of laser instrumentation and different analytical protocols to those used in the present study. The lower $\delta^{18}O$ values reported by Folco et al. (2004) may reflect incomplete reaction of sample material during fluorination.

Ten of the H chondrites analysed by Clayton et al. (1991) were also run in the present study. Multiple aliquots of Forest Vale run by Clayton et al. (1991) gave very different results and so this sample has been excluded. Comparing the remaining 9 samples, the Clayton et al. (1991) mean $\delta^{18}O$ value is displaced by 0.19‰ towards lighter values compared to the same samples analysed in this study. A significant part of this difference relates to Forest City, for which Clayton et al. (1991) report a $\delta^{18}O$ value of 3.63‰, whereas the value determined in this study is 4.67‰. If this sample is excluded from the comparison, the difference between the two studies becomes only 0.08‰, again with the Clayton et al. (1991) data displaced to lighter values. In terms of $\Delta^{17}O$ values, the Clayton et al. (1991) samples are on average displaced to lower values by 0.01‰ compared to the same samples run in this study.

5. DISCUSSION

Of all the iron meteorite groups, the IIEs are arguably the most complex and enigmatic. In common with other silicated irons, the formation of IIEs is problematic due to the large density contrast that exists between molten metal and silicate, such that unmixing should have taken place rapidly, possibly on timescales of months (Wasson and Wang, 1986). In addition, and in marked contrast to the relatively homogeneous composition of inclusions in the IABs, silicate inclusions in the IIEs display a compositional and textural diversity unique amongst iron meteorite groups (Mittlefehldt et al., 1998). In this section we look first at the various lines of evidence that help to constrain the origin of the IIEs before presenting a model for their formation.

5.1. Oxygen isotope constraints on the relationship between H chondrites and IIE irons

High precision oxygen isotope data for the IIE silicate inclusions and H chondrites show a clear overlap when plotted on a diagram of $\Delta^{17}O$ vs. $\delta^{18}O$ (Fig. 2). Such an overlap suggests that both may be derived from a common oxygen isotopic reservoir and are therefore in some way genetically related. However, such a relationship does not imply that all the H chondrites and all of the IIE silicate inclusions were originally derived from a single source i.e. a single H chondrite-IIE parent asteroid. Recent work by Vernazza et al. (2014) indicates that large compositionally similar asteroids may be a natural consequence of planetesimal formation. They found that several asteroid families spectrally matched both the H and LL chondrites and inferred that meteorites from a given ordinary chondrite class can originate from multiple parent bodies. Therefore, a single asteroidal source for all the H chondrites may not be realistic. In the case of the IIE irons, the silicate inclusions may be derived from H or HH chondrite-like material that is related to, but not necessarily directly derived from, the source or sources that currently supply H chondrite meteorites to Earth. This distinction may be important when attempting to interpret the oxygen isotope relationships revealed in this study.

The 2σ variation on the overall H chondrite average ($\Delta^{17}O = 0.70 \pm 0.08$‰ (2σ); $\delta^{18}O = 4.17 \pm 0.42$‰ (2σ)) (Table 7) shows a significant degree of overlap with the bulk analyses for the differentiated IIE inclusions (Fig. 2). However, Colomera plots well outside the 2σ range of the H chondrites (Fig. 2) at higher $\Delta^{17}O$ values, whereas in contrast the primitive chondritic inclusions plot at significantly lower $\Delta^{17}O$ values (Fig. 2). This variation could be interpreted as indicating that the Colomera inclusions sample material derived from an alternative precursor, such as the L chondrites. In contrast, the primitive chondritic IIE

Table 5
Results of two pyroxene geothermometry calculations using QUILF (Andersen et al., 1993).

	OPX			CPX		Temp °C	Uncertainty
	Fs	En	Wo	En	Wo		
Watson	0.169	0.795	0.036	0.513	0.399	1100	36
Miles	0.208	0.764	0.028	0.5	0.394	1029	22
Weekeroo St.	0.358	0.602	0.04	0.445	0.39	1017	76
Tarahumara	0.211	0.759	0.03	0.471	0.42	1028	17
Elga				0.471	0.431		
Colomera	0.184	0.804	0.012	0.452	0.436	860	99
Kodaikanal	0.182	0.802	0.016				

Table 6
High precision oxygen isotopic analyses for silicate inclusions and mineral separates from 11 IIE iron meteorites.

IIE Inclusions	Sub-type	N	$\delta^{17}O‰$	2σ	$\delta^{18}O‰$	2σ	$\Delta^{17}O‰$	2σ	$\Delta^{17}O‰_{linear}$	2σ
Colomera (Diopside)	Differentiated	2	3.02	0.14	4.08	0.2	0.90	0.04	0.88	0.04
Colomera (Feldspar)	Differentiated	2	3.54	0.02	5.11	0.08	0.88	0.06	0.86	0.03
Garhi Yasin	Chondritic	1	2.91		4.48		0.58		0.56	
Kodaikanal (Augite)	Differentiated	2	2.98	0.06	4.22	0.08	0.79	0.02	0.77	0.02
Kodaikanal (Alkali Glass)	Differentiated	1	2.95		4.25		0.74		0.72	
Kodaikanal (Glass)	Differentiated	1	3.69		5.62		0.77		0.74	
Miles	Differentiated	2	3.90	0.04	6.25	0.12	0.65	0.02	0.62	0.02
Miles (Feldspar)	Differentiated	1	3.37		5.22		0.66		0.63	
Netschaëvo	Chondritic	2	2.18	0.06	3.06	0.12	0.59	0.00	0.57	0.00
NWA 5608	Differentiated	1	3.01		4.45		0.70		0.68	
Tarahumara	Differentiated	2	2.95	0.1	4.15	0.18	0.79	0.00	0.77	0.00
Techado	Chondritic	2	3.05	0.12	4.74	0.16	0.59	0.04	0.56	0.04
TYR 05181	Differentiated	2	2.45	0.18	3.52	0.36	0.62	0.00	0.60	0.00
Watson 001	Chondritic, evolved	9	3.09	0.28	4.53	0.60	0.73	0.14	0.71	0.14
Weekeroo Sta.	Differentiated	4	2.83	0.38	4.18	0.68	0.66	0.06	0.64	0.06
Weekeroo Sta. (Feldspar)	Differentiated	2	3.69	0.30	5.88	0.50	0.63	0.04	0.61	0.04
Mean values			**3.10**	**0.90**	**4.61**	**1.68**	**0.70**	**0.20**	**0.68**	**0.20**
Mean values (single analysis per sample)			**3.00**	**0.82**	**4.45**	**1.44**	**0.69**	**0.20**	**0.67**	**0.20**

Table 7
High precision oxygen isotopic analyses for 20 H chondrites.

		N	$\delta^{17}O‰$	2σ	$\delta^{18}O‰$	2σ	$\Delta^{17}O‰$	2σ	$\Delta^{17}O‰_{linear}$	2σ
Dhajala	H3.8	4	2.82	0.32	4.21	0.40	0.63	0.12	0.61	0.12
Ankober	H4	2	3.08	0.02	4.53	0.04	0.73	0.00	0.71	0.00
Bath	H4	2	2.96	0.02	4.35	0.06	0.70	0.02	0.68	0.02
Forest Vale	H4	4	2.78	0.06	4.00	0.08	0.70	0.02	0.68	0.02
Quenggouk	H4	2	2.88	0.04	4.03	0.02	0.78	0.02	0.76	0.02
Seres	H4	2	3.04	0.00	4.43	0.04	0.73	0.02	0.71	0.02
Allegan	H5	4	2.77	0.18	4.03	0.28	0.67	0.04	0.66	0.04
Ambapur Nagla	H5	2	2.86	0.06	4.10	0.12	0.73	0.00	0.71	0.00
Beaver Creek	H5	2	2.93	0.04	4.27	0.06	0.71	0.00	0.69	0.00
Castalia	H5	2	2.90	0.14	4.12	0.18	0.76	0.0	0.74	0.06
Forest City	H5	1	3.18		4.67		0.75		0.73	
Jilin	H5	2	2.74	0.18	3.83	0.36	0.75	0.00	0.73	0.00
Lost City	H5	2	2.81	0.04	3.97	0.00	0.74	0.02	0.72	0.02
Pantar	H5	2	2.86	0.20	4.11	0.36	0.72	0.02	0.70	0.02
Pribram	H5	2	2.92	0.02	4.18	0.08	0.75	0.02	0.73	0.02
Rose City	H5	6	2.64	0.14	3.88	0.28	0.62	0.02	0.61	0.02
Canon City	H6	2	2.93	0.16	4.15	0.24	0.77	0.04	0.75	0.04
Guarena	H6	4	2.97	0.16	4.24	0.26	0.76	0.02	0.74	0.02
Portales Valley	H6	2	2.85	0.22	4.09	0.42	0.72	0.00	0.70	0.00
Queens Mercy	H6	2	2.86	0.10	4.11	0.16	0.72	0.00	0.71	0.00
Average			**2.89**	**0.24**	**4.17**	**0.42**	**0.72**	**0.08**	**0.70**	**0.08**
Average H4-H6			**2.89**	**0.26**	**4.16**	**0.42**	**0.73**	**0.08**	**0.71**	**0.08**

inclusions may have originated from a HH-like chondrite parent body. However, this interpretation is based on a comparison with a dataset of 20 H chondrites and so may be an underrepresentation of the oxygen isotopic variation present in the H chondrite population as a whole.

In Fig. 3, the 2σ variation of the H chondrite mean obtained in this study is compared to that of Clayton et al. (1991). Also shown is the 2σ variation for L chondrites obtained by Clayton et al. (1991). As is clear from Fig. 3, the variation obtained by Clayton et al. (1991) for the H chondrites with respect to $\Delta^{17}O$ is significantly greater than was measured in the present study. When referenced to the Clayton et al. (1991) data, both Colomera and the primitive chondritic IIEs all fall within the H chondrite field and in the case of Colomera outside the field of L chondrites. It could be argued that the relatively large size of the equilibrated H chondrite field obtained by Clayton et al. (1991) reflects lower levels of analytical precision, the sample size ($n = 23$) being only slightly greater than in this study ($n = 20$). However, the two sample sets are not identical. In addition, higher precision measurements of L chondrites are unlikely to cause Colomera to plot in the L chondrite field. Despite the fact that Colomera lies outside the field of H chondrites measured in this study

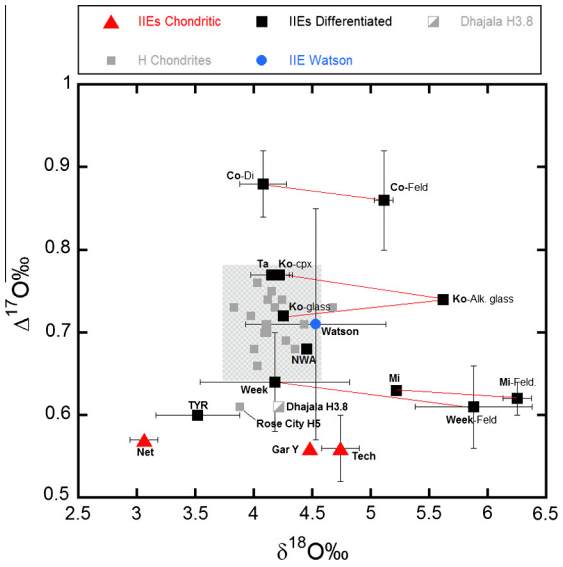

Fig. 2. Oxygen isotopic compositions of silicate inclusions in IIE irons and H chondrites. All error bars are ±2σ. Tie lines connect mineral separates (labelled) and bulk analyses for individual IIE samples. Abbreviations: Co–Colomera; Gar Y–Garhi Yasin; Ko – Kodaikanal; Mi – Miles; Net – Netschaëvo; NWA – NWA 5608; Ta – Tarahumara; Tech – Techado; TYR – TYR 05181; Watson – Watson 001; Week – Weekeroo Station. Mineral separates: Feld – feldspar, Di – Diopside, Alk. glass – alkali glass. Data points for IIE samples without a phase label represent bulk analyses. IIE data points without error bars represent single analyses. Hatched box shows ±2σ variation for H chondrite analyses.

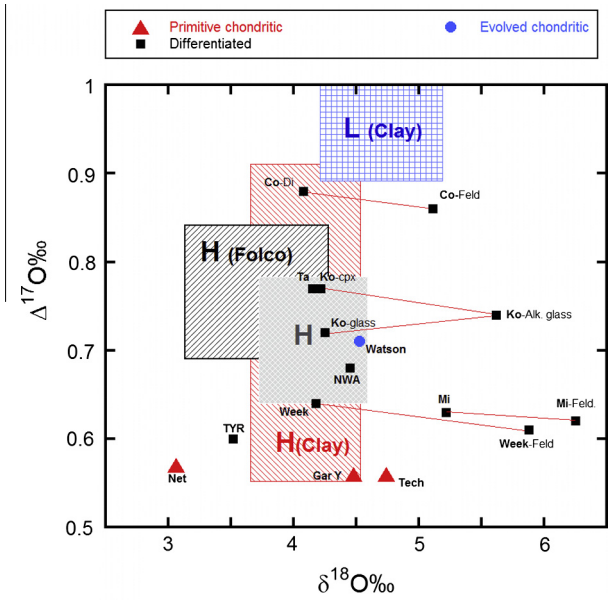

Fig. 3. Oxygen isotopic composition of silicate inclusions in IIE irons compared to H and L chondrites. Symbols and abbreviations as in Fig. 2. Grey hatched box shows 2σ range for H chondrite analyses from this study. Red box with diagonal lines shows 2σ range for H chondrite analyses by Clayton et al. (1991). Blue chequered box shows lower part of the 2σ range for L chondrite analyses by Clayton et al. (1991). Black box with diagonal lines shows the 2σ range for H chondrite analyses by Folco et al. (2004). (For interpretation of the references to colour in this figure legend, the reader is referred to the web version of this article.)

(Fig. 2), the chemical and mineralogical characteristics of Colomera's inclusions are very similar to those of Elga, for example, so they are probably derived from the same source.

Olivine compositions in the primitive chondritic IIEs Netschaëvo, Techado and Mont Dieu are slightly more reduced than is observed in normal H chondrites (Mittlefehldt et al., 1998; Van Roosbroek et al., 2015; this study). In the case of Netschaëvo it was suggested by Bild and Wasson (1977) that silicate material in this meteorite represents a distinct type of FeO-poor ordinary chondrite. The fact that all of the primitive chondritic IIEs analysed in this study have anomalously low $\Delta^{17}O$ values (Fig. 3) could be taken as evidence in support of their derivation from precursor material that is distinct to that which was parental to the more evolved IIEs. However, the oxygen isotope composition of the primitive chondritic IIE Mont Dieu measured in the recent study of Van Roosbroek et al. (2015) places it well within the range of differentiated IIEs and apart from the primitive IIEs measured in this study. In addition, Netschaëvo samples were forged to temperatures as high as 1000 °C (Buchwald, 1975), which might potentially have caused reduction of its silicates and also disturbance of its oxygen isotope composition. However, neither Techado or Garhi Yasin have been forged in a similar manner to Netschaëvo and consequently it would appear likely that at least some primitive chondritic IIEs formed from precursor material that was more reduced than H chondrites, possibly equivalent to the low FeO ordinary chondrites, also known as HH chondrites (McCoy et al., 1994; Russell et al., 1998; Troiano et al., 2011; Yamaguchi et al., 2015).

In summary, the oxygen isotope variations displayed by the IIE silicates provide strong evidence that their parent source material was isotopically heterogeneous and closely related to the H and HH chondrites. The differentiated IIE irons show clear compositional overlap with the H chondrites, whereas at least some of the primitive chondritic IIEs seem to have sampled material that was more reduced than H chondrites and had lower $\Delta^{17}O$ values. This tendency for more reduced chondrites to have lower $\Delta^{17}O$ values is also shown by H chondrites (Rubin, 2005), and some HH chondrites (McCoy et al., 1994; Russell et al., 1998; Yamaguchi et al., 2015). This trend may reflect the addition of isotopically heavy oxygen in phyllosilicates or water prior to metamorphism (Rubin, 2005; Kita et al., 2010). We do not exclude the possibility that some H or HH chondrites are derived from the same body that supplied us with the IIE iron meteorites.

5.2. Compositional diversity of the IIE parent body

As discussed in Section 5.1, the IIEs as a whole show a wide variation in $\Delta^{17}O$ values. This is in marked contrast to the differentiated achondrites, including Martian meteorites (Franchi, 2008), lunar basalts (Hallis et al., 2010), main-group pallasites (Greenwood et al., 2013), and HEDs (Greenwood et al., 2005), which experienced large-scale

melting and isotopic homogenisation, possibly as a result of the formation of magma oceans. The IIE parent body was heterogeneous and did not experience a significant degree of melting and isotopic equilibration.

Compared to the chondritic IIE inclusions, the differentiated silicates in IIEs have experienced a higher degree of thermal processing and differentiation, which resulted in fractionated chemical compositions (Burnett and Wasserburg, 1967a; Ruzicka et al., 1999; Takeda et al., 2003). All the IIEs with differentiated silicates show similar mineralogies and consist predominantly of orthopyroxene, clinopyroxene, and Na-rich feldspar, with some inclusions containing K-rich glass and crystals. One of the major differences between the chondritic and differentiated IIE silicates is the volume of metal located within the silicate inclusions, with the chondritic inclusions having a much greater volume of metal (>10 vol%) compared to the differentiated inclusions which is often <1 vol%) (Ruzicka, 2014). The reduced metal content of the differentiated inclusions demonstrates that they experienced temperatures well above initial FeS–FeNi metal melting ~980 °C (Hutchison, 2004). Their fractionated compositions and melted textures are indicative of temperatures that exceeded the silicate solidus, ~1050 °C (Hutchison, 2004). Peak temperatures experienced by material of the primitive chondritic subtype would have been lower than either that of the evolved chondritic or differentiated subtypes. Assuming that the impact that mixed metal and silicate did not heat them, the IIE parent body was probably thermally stratified, possibly with a relatively cool exterior (primitive chondritic subtype) and a hotter partially melted interior (differentiated subtypes). Loss of metal and sulphide from the differentiated subtypes suggests that metal may have partly separated into a core.

Individual IIE meteorites do not show a diversity of inclusion types, i.e. primitive chondritic and differentiated subtypes are never intermixed in a single meteorite. This suggests that they formed in separate locations in the original IIE parent body. This lack of intermixing in individual IIE specimens also suggests that metal and silicate were not simply mixed by a hypervelocity impact that created an impact melt pool. In the next section we look at the composition of IIE iron metal and what this might indicate about the formation conditions of its silicate inclusions.

5.3. IIE metal compositions

Concentrations of trace elements, especially Ir, in IIE irons are relatively homogeneous compared to those of the magmatic irons, showing that they did not form by fractional crystallization of a metallic pool or core (Wasson and Wang, 1986; Wasson and Scott, 2011). There are small chemical variations within IIE irons but they resemble those in IAB iron meteorites and may reflect limited solid–liquid fractionation during melting or solidification (Wasson and Scott, 2011). Wasson and Wang (1986) inferred from their study that IIE irons and their silicate inclusions formed in impact melt pools on the surface of a chondritic body.

Luais (2007) analyzed the Ge isotopic composition of five IIE irons and found that most had $^{74}Ge/^{70}Ge$ ratios that were much lighter than those in other irons. She inferred that the Ge isotopic variations in IIE metal were due to evaporative losses during impact heating, which raised the $^{74}Ge/^{70}Ge$ ratio. However, the two meteorites with the highest $^{74}Ge/^{70}Ge$ ratios, Watson and Mont Dieu, have chondritic silicates and the two meteorites with the lowest $^{74}Ge/^{70}Ge$ ratios, Miles and Weekeroo Station, have differentiated silicates. Therefore processing of chondritic material by impacts cannot readily account for both the Ge isotopic variation and the fractionation displayed by IIE silicate inclusions.

As discussed in Section 5.1, oxygen isotope evidence supports a genetic relationship between the IIE inclusions and the H chondrites, although not necessarily a single asteroidal source for both. However, if the IIEs and H chondrites are derived from a single parent body then the metal in both should exhibit strong compositional similarities. Teplyakova et al. (2012) analysed the metal in five IIE irons and showed that it did not match the composition of metal in H chondrites. They inferred that IIE metal did not form by quenching of metal from an impact melt pool on an H chondrite body and favoured a more reduced precursor material.

5.4. Metal–silicate mixing

The major event in the formation of the IIE irons was the mixing of metal and silicate materials. In keeping with the majority of previous studies (see summary in Ruzicka, 2014), it is difficult not to view this as having taken place in response to an impact event, although models invoking internal processes have also been proposed (Wasserburg et al., 1968; McCoy, 1995).

As discussed above, Wasson and Wang (1986) suggested that the IIE irons originated as individual pools of impact-melt formed by hypervelocity projectiles near the near-surface region of a chondritic parent body. Impact modelling studies by Davison et al. (2012, 2013) and Ciesla et al. (2013) indicate that significant localized heating could have taken place close to the point of impact in a target body, especially one with significant porosity. However, the impact-melt model of Wasson and Wang (1986) has been criticised by Keil et al. (1997) who suggested that partial melting of the type required to explain the origin of metal melt pools and silicate partial melts on the IIE parent body is not explicable in terms of impact heating of asteroids by hypervelocity shock. They argue that either total melting would occur in the most energetic situations, or alternatively, melting would be too localized to account for the formation of metal melt pools. More recently, Tomkins et al. (2013) have suggested that impact processes may have caused metal segregation by a process of deformation-induced melt migration. These authors point to evidence such as entrainment of angular silicate material within masses of FeNi metal seen in meteorites such as the H chondrite Portales Valley and the IIE irons with chondritic inclusions as evidence that this represents a viable process.

In contrast to hypervelocity impacts, a number of studies suggest that hit-and-run style collisions were commonplace during accretion in the early solar system (Asphaug et al., 2006; Asphaug and Reufer, 2014). A consequence of these low-velocity encounters is that the crust and mantle can be almost completely removed from the smaller of the two colliding bodies, leaving what is essentially a denuded iron-rich core. One possibility is that the IIE irons formed as a result of an impact between such an iron-rich body and a larger H chondrite-related parent asteroid. However, the chemical composition of IIE metal does not appear to match this model (Wasson and Scott, 2011; Teplyakova et al., 2012).

Group IIE irons probably formed on a single H/HH chondrite-like body that was heated above ~900 °C by ^{26}Al decay rather than by impact heating. If the impact that mixed metal and silicate did not supply significant heat, then group IIE irons may have formed by impact mixing of pre-existing pools of molten metal and partly melted silicates. In this case, rapid cooling of molten metal to trap silicates may have resulted from disruption by a hit-and-run impact.

5.5. Age constraints

Dating studies indicate that the IIEs have experienced a complex formational history. W isotopic measurements of metal from six IIE meteorites are consistent with three consecutive metal segregation events at ~3, ~13 and ~28 Ma after CAI formation (Schulz et al., 2012). It was suggested that while the first event could be interpreted as resulting from internal radiogenic heating, the latter two are most likely a result of impact processes. This would be consistent with the melt pool model of Wasson and Wang (1986).

A variety of long-lived radioisotopic dating techniques have been applied to the IIE irons. These include Ar–Ar (Niemeyer, 1980; Bogard et al., 2000; Bogard, 2011), K–Ar (Bogard et al., 1968; Olsen et al., 1994; Casanova et al., 1995), Rb–Sr (Sanz et al., 1970; Burnett and Wasserburg, 1967a,b; Evensen et al., 1979), Sm–Nd (Snyder et al., 2001), Pb–Pb (Göpel et al., 1985), Re–Os (Birck and Allègre, 1998) and I–Xe dating (Niemeyer, 1980; Brazzle et al., 1999). These studies have identified two distinct age groups for the IIE silicate inclusions, generally referred to as the old age group and the young age group (Mittlefehldt et al., 1998; Bogard et al., 2000). The old age group of Colomera, Miles, Tarahumara, Techado, and Weekeroo Station have ages of 4.3–4.5 Ga. The young age group of Kodaikanal, Netschaëvo, and Watson have ages of 3.5–3.8 Ga. Both groups contain meteorites with chondritic as well as differentiated silicate inclusions. The young age group were probably reheated by a major impact at 3.7 Ga, which caused severe deformation of the Widmanstätten pattern and impact melting of phosphide in Kodaikanal and Watson (Buchwald, 1975; Olsen et al., 1994). Impact deformation intense enough to melt schreibersite is so rare that another occurrence in the IIE iron, Verkhne Dnieprovsk, (Buchwald and Clarke, 1987) probably formed at the same time. The high fraction of IIE irons that recorded the late heavy bombardment implies a relatively large parent body (Bogard, 2011). Our oxygen isotope data (Fig. 2) show no significant oxygen isotope differences between the young and old groups implying that all IIE irons may come from a single large asteroid or asteroid family.

Cosmic-ray exposure ages of IIE irons have been determined from metal and silicate inclusions using several techniques including ^{3}He, ^{21}Ne and ^{38}Ar. The three young age iron meteorites have relatively short exposure ages of 1–15 Ma (Olsen et al., 1994; Bogard et al., 2000). The exposure age of Watson of 8 Ma coincides with the 6–10 Ma age shown by roughly half the H chondrites (Marti and Graf, 1992; Olsen et al., 1994; Graf and Marti, 1995). This could be taken as evidence for a common source, as Olsen et al. (1994) argued. However, acapulcoites and lodranites, which are closely related to one another, but unrelated to H chondrites, all have exposure ages of 5–10 Ma. Terribilini et al. (2000) suggest that this seemingly high collisional activity at 5–10 Ma may reflect the passage through the asteroid belt of numerous projectiles, possibly from the destruction of another asteroid.

Four IIE irons with old radiometric ages of ~4.3 Ga have much longer cosmic ray exposure ages: 30–100 Ma for Techado and Colomera (Casanova et al., 1995; Bogard et al., 2000) and around 100–600 Ma for Weekeroo Station and Miles (see Bogard et al., 2000). The difference in exposure ages between the young and old IIE iron meteorites suggests that they are derived either from separate regions of the same parent body (Bogard et al., 2000), or from separate bodies (Niemeyer, 1980). However, petrographic and isotopic similarities between the two age groups favour a common precursor asteroid, even if it was subsequently disrupted into two or more daughter bodies.

5.6. A formation model for the IIE iron meteorites

5.6.1. Constraints

A successful formation model for the IIEs should account for the following constraints, which are based on properties of the IIE irons that were discussed above.

- The group IIE irons are isotopically heterogeneous, as shown by the range in Δ^{17}O values of the IIE silicates ($\geqslant$0.31‰). The H chondrites are more homogeneous and it seems unlikely that both groups come from a single body. However, it is possible, perhaps likely, that some H or HH chondrites are derived from the same body that supplied us with IIE irons.
- The group IIE parent body accreted from ordinary chondrite material that resembled H and HH chondrites as shown by the presence of chondrules within some chondritic inclusions, the overall similarity in petrology, texture, and oxygen isotopic compositions of IIE silicates and H chondrites, and the presence of silicates with low Δ^{17}O values and FeO concentrations.
- Prior to metal–silicate mixing, the parent body probably had a hot interior due to ^{26}Al heating and a cool exterior. Either the silicate mantle was partly molten before impact mixing, or else the impact that mixed metal or silicate caused localized silicate melting.

- After metal–silicate mixing, rapid cooling and crystallization of molten metal prevented silicate globules from separating gravitationally. If the silicates were partly melted prior to impact the parent body must have been disaggregated into small chunks so that the metal–silicate mixture cooled rapidly. Alternatively, rapid crystallization may have resulted from localized formation of impact-generated veins of metal–silicate melt with diverse widths. The absence of silicates in one-third of the IIE irons shows that some meter-sized volumes of molten metal crystallized less rapidly so that silicates were not trapped in metal.
- If the deep interior of the parent asteroid was differentiated prior to metal–silicate mixing, unknown selection processes must have conspired to prevent metal-free rock from reaching us in the form of IIE-related achondrites. The absence of these achondrites can be understood more readily if the parent body was largely undifferentiated and silicate melting was confined to impact-generated veins during the metal–silicate mixing event.
- Two-pyroxene equilibration temperatures of 900–1100 °C indicate rapid cooling below these temperatures. Consistent with the preservation of glass in the fractionated inclusions.
- After this rapid cooling, the IIE irons were deeply buried within a large silicate-rich body so that they cooled slowly below ~700 °C and developed Widmanstätten patterns of oriented kamacite plates in taenite (Buchwald, 1975). A large parent body is also indicated by the significant number of IIE irons that were impact-heated during the late heavy bombardment.
- Chondritic and differentiated inclusions were not intimately mixed on sub-meter scales in IIE irons, but both types were impact-heated during the late heavy bombardment.

Group IIE irons, like many other meteorite types, experienced at least one major collision during the first few Myr after they accreted when they had hot interiors. The impact that created the IIE irons with silicate inclusions probably resembled the impacts that generated IAB irons, Portales Valley, and other H chondrites with metallic veins (Tomkins et al., 2013; Scott et al., 2014). Group IIE irons with differentiated inclusions appear to have formed by similar processes to those that affected the Sombrerete and Guin ungrouped irons and the IAB complex iron, Caddo County, as they contain differentiated inclusions with similar compositions (Ruzicka, 2014). Metal and silicates in IIE irons were mixed together but not intimately as in the Caddo County iron, which contains both chondritic and differentiated inclusions (Benedix et al., 2000; Ruzicka, 2014).

5.6.2. A model for the formation of IIE iron meteorites

Based on the evidence presented in this study, a model for the formation of the IIE irons is described below which attempts to account for the principal features of the IIE iron meteorites outlined above. This model is an extension of the IIE model proposed by Ruzicka (2014).

1. The IIE parent body may have accreted relatively late compared to those bodies that were the source of the magmatic iron meteorites. Hence, it underwent initial heating and incipient differentiation driven by the decay of short-lived radionuclides, such as ^{26}Al. However, heating was insufficient to cause isotopic homogenization.
2. Prior to large-scale segregation of the siderophiles and lithophiles due to the internal heating the body experiences a major hit-and-run style collision. This would have induced melting of the silicates near the deformation zone and melt migration would have trapped silicate globules within the molten metal. This is based on the model of Tomkins et al. (2013). Metal and silicate were mixed in such a way that chondritic and differentiated silicates from different zones in the original body were not completely mixed together and so are not both present within a single meteorite.
3. While there is evidence from dating studies to support multiple metal–silicate mixing events on the IIE parent body we see this as being a fairly improbable scenario. The most likely source of molten metal on the IIE parent body was segregation during initial radiogenic heating, or alternatively melt production from a disruptive impact event. Once molten metal and silicate material were catastrophically brought together an initial phase of rapid cooling must have taken place to prevent silicate–metal unmixing. It seems unlikely that later local scale impacts would reproduce repeatedly and almost exactly the same textural relationships. The later dates recorded by W isotope dating studies probably represent resetting events.
4. At the close of the event that caused metal–silicate mixing a deep fragmental regolith formed on the IIE parent body resulting in significantly slower cooling rates consistent with the evidence from cooling rate studies of IIE metal.
5. After cooling the body was impacted at least one further time, resetting the ages of this region and so forming the "Young" IIE meteorite samples at about 3.7 Ga. This event could have caused the fragmentation of the IIE parent body into at least two daughter asteroids. Rapid heating followed by fast cooling during late impacts probably accounts for the transformation of feldspar-rich materials into glass.

6. SUMMARY AND CONCLUSIONS

The silicate-bearing IIEs are arguably the most complex and enigmatic of all iron meteorite groups. In order to understand their origin we have undertaken a detailed oxygen isotope investigation of IIE silicate inclusions. In addition, we have studied the petrography and mineral chemistry of selected inclusions. Based on petrographic and textural evidence, a fourfold classification scheme for the silicate-bearing IIEs is proposed: (1) primitive chondritic, (2) evolved chondritic, (3) differentiated with >10 vol.% orthopyroxene, and (4) differentiated with <10 vol.% orthopyroxene. Oxygen isotope analysis of 20

H chondrites demonstrates a close genetic link with the IIEs. However, the significantly greater variation with respect to $\Delta^{17}O$ observed in the IIEs compared to our H chondrite analyses suggests that both groups may not be derived from a single common parent body. The IIEs may represent material derived from an H/HH parent body, distinct from that which currently supplies the H chondrite meteorite population. The formation of the IIEs is best explained by a model involving an internally heated H/HH chondrite-like body that experienced only the initial stages of differentiation prior to disruption during a major hit-and-run style collision that resulted in silicate–metal mixing. The initial stages of this event involved a phase of rapid cooling that prevented unmixing of metal and silicates. Reassembly of the IIE parent body produced a large regolith blanket that facilitated subsequent slow cooling. The IIE parent body has probably experienced numerous subsequent less catastrophic collisions.

ACKNOWLEDGEMENTS

We are grateful to Jenny Gibson for all her help with the oxygen isotopic analyses and to Deon Van Niekerk for completing the pyroxene thermometry calculations. We thank John Wasson, Dimitri Papanastassiou, and two anonymous reviewers for their helpful and constructive comments and suggestions. Finally, we would like to thank all the institutions that provided the samples for analysis named in Table 2. We are particularly grateful to Dr Caroline Smith from the Natural History Museum, London; Dr Linda Welzenbach of the Smithsonian Institution, National Museum of Natural History, Washington; Robert Haag, Marvin Kilgore, and Jerry Delaney; Philipp Heck of the Field Museum, Chicago; Adrian Brearley and Lee Ann Lloyd of the University of New Mexico for their help and assistance. The authors wish to thank the Science and Technology Facilities Council, United Kingdom and the Open University Charter for providing funding for this project.

APPENDIX A. SUPPLEMENTARY DATA

Supplementary data associated with this article can be found, in the online version, at http://dx.doi.org/10.1016/j.gca.2015.10.014.

REFERENCES

Andersen D. J., Lindsley D. H. and Davidson P. M. (1993) QUILF: a Pascal program to assess equilibria among Fe–Mg–Mn–Ti oxides, pyroxenes, olivine, and quartz. *Comp. Geosci.* **19**, 1333–1350.

Asphaug E. and Reufer A. (2014) Mercury and other iron-rich planetary bodies as relics of inefficient accretion. *Nature Geosci.* **7**, 564–568.

Asphaug E., Agnor C. B. and Williams Q. (2006) Hit-and-run planetary collisions. *Nature* **439**, 155–160.

Bence A. E. and Burnett D. S. (1969) Chemistry and mineralogy of the silicate and metal of Kodaikanal meteorite. *Geochim. Cosmochim. Acta* **33**, 387–407.

Benedix G. K., McCoy T. J., Keil K. and Love S. G. (2000) A petrologic study of the IAB iron meteorites: constraints on the formation of the IAB-winonaite parent body. *Meteorit. Planet. Sci.* **35**, 1127–1141.

Benedix G. K., Lauretta D. S. and McCoy T. J. (2005) Thermodynamic constraints on the formation conditions of winonaites and silicate-bearing IAB irons. *Geochim. Cosmochim. Acta* **69**, 5123–5131.

Bild R. W. and Wasson J. T. (1977) Netschaëvo: a new class of chondritic meteorite. *Science* **197**, 58–62.

Birck J. L. and Allègre C. J. (1998) ^{187}Re–^{187}Os in iron meteorites and the strange origin of the Kodaikanal meteorite. *Meteorit. Planet. Sci.* **33**, 647–653.

Bizzarro M., Baker J. A., Haack H. and Lundgaard L. (2005) Rapid timescales for accretion and melting inferred from ^{26}Al–^{26}Mg chronometry. *Astrophys. J.* **632**, L41–L44.

Bogard D. D. (2011) K-Ar ages of meteorites: clues to parent-body thermal histories. *Chem. Erde* **71**, 207–226.

Bogard D., Burnett D., Eberhardt P. and Wasserburg G. J. (1968) ^{40}Ar–^{40}K ages of silicate inclusions in iron meteorites. *Earth Planet. Sci. Lett.* **3**, 275–283.

Bogard D. D., Garrison D. H. and McCoy T. J. (2000) Chronology and petrology of silicates from IIE iron meteorites: evidence of a complex parent body evolution. *Geochim. Cosmochim. Acta* **64**, 2133–2154.

Brazzle R. H., Pravdivtseva O. V., Meshik A. P. and Hohenberg C. M. (1999) Verification and interpretation of the I-Xe chronometer. *Geochim. Cosmochim. Acta* **63**, 739–760.

Buchwald V. F. (1975) *Handbook of Iron Meteorites*. Univ. California Press.

Buchwald V. F. and Clarke R. S. (1987) The Verkhne Dnieprovsk iron meteorite specimens in the Vienna collection and the confusion of Verkhne Dnieprovsk with Augustinovka. *Meteoritics* **22**, 121–135.

Bunch T. E., Keil K. and Olsen E. (1970) Mineralogy and petrology of silicate inclusions in iron meteorites. *Contrib. Mineral. Petrol.* **25**, 240–297.

Burnett D. S. and Wasserburg G. J. (1967a) ^{87}Rb– ^{87}Sr ages of silicate inclusions in iron meteorites. *Earth Planet. Sci. Lett.* **2**, 397–408.

Burnett D. S. and Wasserburg G. J. (1967b) Evidence for the formation of an iron meteorite at 3.8×10^9 years. *Earth Planet. Sci. Lett.* **2**, 137–147.

Casanova I., Graf T. and Marti K. (1995) Discovery of an unmelted H- chondrite inclusion in an iron meteorite. *Science* **268**, 540–542.

Chabot N. L. and Haack H. (2006) Evolution of asteroidal cores. In *Meteorites and the early solar system II*. University of Arizona Press, pp. 747–771.

Ciesla F. J., Davison T. M., Collins G. S. and O'Brien D. P. (2013) Thermal consequences of impacts in the early solar system. *Meteorit. Planet. Sci.* **48**, 2559–2576.

Clayton R. N. and Mayeda T. K. (1963) The use of bromine pentafluoride in the extraction of oxygen from oxides and silicates for isotopic analysis. *Geochim. Cosmochim. Acta* **27**, 43–52.

Clayton R. N. and Mayeda T. K. (1996) Oxygen isotope studies of achondrites. *Geochim. Cosmochim. Acta* **60**, 1999–2017.

Clayton R. N., Mayeda T. K., Goswami J. and Olsen E. J. (1991) Oxygen isotope studies of ordinary chondrites. *Geochim. Cosmochim. Acta* **55**, 2317–2337.

Davison T. M., Ciesla F. J. and Collins G. S. (2012) Post-impact thermal evolution of porous planetesimals. *Geochim. Cosmochim. Acta.* **95**, 252–269.

Davison T. M., O'Brien D. P., Ciesla F. J. and Collins G. S. (2013) The early impact histories of meteorite parent bodies. *Meteorit. Planet. Sci.* **48**, 1894–1918.

Ebihara M., Ikeda Y. and Prinz M. (1997) Petrology and chemistry of the Miles IIE iron: II. Chemical characteristics of the Miles silicate inclusions. *Antarct. Meteorite Res.* **10**, 373–388.

Evensen N. M., Hamilton P. J., Harlow G. E., Klimentidis R., O'Nions R. K. and Prinz M. (1979). Silicate inclusions in Weekeroo Station: Planetary differentiates. *Lunar Planet. Sci. X*. Lunar Planet. Inst., Houston. #376-378(abstr).

Folco L., Bland P. A., D'Orazio M., Franchi I. A., Kelley S. P. and Rocchi S. (2004) Extensive impact melting on the H-chondrite parent asteroid during the cataclysmic bombardment of the early solar system: evidence from the achondritic meteorite Dar al Gani 896. *Geochim. Cosmochim. Acta* **68**, 2379–2397.

Franchi I. A. (2008) Oxygen isotopes in asteroidal materials. In *Oxygen in the Solar System. Rev. Mineral.* **68**, 345–397.

Gaffey M. J. and Gilbert S. L. (1998) Asteroid 6 Hebe: the probable parent body of the H type ordinary chondrites and the IIE iron meteorites. *Meteorit. Planet. Sci.* **33**, 1281–1295.

Goldstein J. I., Scott E. R. D. and Chabot N. L. (2009) Iron meteorites: crystallization, thermal history, parent bodies, and origin. *Chem. Erde* **69**, 293–325.

Göpel C., Manhès G. and Allègre C. J. (1985) Concordant 3,676 Myr U-Pb formation age for the Kodaikanal iron meteorite. *Nature* **317**, 341–344.

Graf T. and Marti K. (1995) Collisional history of H chondrites. *J. Geophys. Res. Planets* **100**(E10), 21247–21263.

Greenwood R. C., Franchi I. A., Jambon A. and Buchanan P. C. (2005) Widespread magma oceans on asteroidal bodies in the early solar system. *Nature* **435**, 916–918.

Greenwood R. C., Barrat J-A., Scott E. R. D., Franchi I. A., Yamaguchi A., Gibson J. M., Haack H., Lorenz C. A., Ivanova M. A., and Bevan A. (2013) Large-scale melting and impact mixing on early-formed asteroids: Evidence from high-precision oxygen isotope studies. *Lunar Planet. Sci. XLIV*. Lunar Planet. Inst., Houston. #3048 (abstr).

Haack H. and McCoy T. J. (2003) Iron and stony-iron meteorites. In *Treatise on geochemistry*, vol. 1 (ed. A. M. Davis), pp. 325–346. Meteorites, Comets and Planets. Oxford, Elsevier.

Hallis L. J., Anand M., Greenwood R. C., Miller M. F., Franchi I. A. and Russell S. S. (2010) The oxygen isotope composition, petrology and geochemistry of mare basalts: evidence for large-scale compositional variation in the lunar mantle. *Geochim. Cosmochim. Acta* **74**, 6885–6899.

Hutchison R. (2004) *Meteorites: A Petrologic*. Cambridge University Press, Chemical and Isotopic Synthesis.

Ikeda Y., Ebihara M. and Prinz M. (1997) Petrology and chemistry of the Miles IIE iron. I: description and petrology of twenty new silicate inclusions. *Antarct. Meteorite Res.* **10**, 355–372.

Keil K., Stöffler D., Love S. G. and Scott E. R. D. (1997) Constraints on the role of impact heating and melting in asteroids. *Meteorit. Planet. Sci.* **32**, 349–363.

Kita N. T., Nagahara H., Tachibana S., Tomomura S., Spicuzza M. J., Fournelle J. H. and Valley J. W. (2010) High precision SIMS oxygen three isotope study of chondrules in LL3 chondrites: role of ambient gas during chondrule formation. *Geochim. Cosmochim. Acta* **74**, 6610–6635.

Kleine T., Mezger K., Palme H., Scherer E. and Münker C. (2005) Early core formation in asteroids and late accretion of chondritic parent bodies: evidence from ^{182}Hf-^{182}W in CAIs, metal-rich chondrites, and iron meteorites. *Geochim. Cosmochim. Acta* **69**, 5805–5818.

Kleine T., Touboul M., Bourdon B., Nimmo F., Mezger K., Palme H., Jacobsen S. B., Yin Q.-Z. and Halliday A. N. (2009) Hf-W chronology of the accretion and early evolution of asteroids and terrestrial planets. *Geochim. Cosmochim. Acta* **73**, 5150–5188.

Kruijer T. S., Touboul M., Fischer-Gödde M., Bermingham K. R., Walker R. J. and Kleine T. (2014) Protracted core formation and rapid accretion of proto planets. *Science* **344**, 1150–1154.

Lindsley D. H. and Andersen D. J. (1983) A two-pyroxene thermometer. *J. Geophys. Res.* **88**, A887–A906.

Luais B. (2007) Isotopic fractionation of germanium in iron meteorites: significance for nebular condensation, core formation and impact processes. *Earth Planet. Sci. Lett.* **262**, 21–36.

Marti K. and Graf T. (1992) Cosmic-ray exposure history of ordinary chondrites. *Ann. Rev. Earth Planet. Sci.* **20**, 221–243.

McCoy T. J. (1995) Silicate-bearing IIE irons: early mixing and differentiation in a core-mantle environment and shock resetting of ages. *Meteoritics* **30**, 542–543 (abstr.).

McCoy T., Keil K., Scott E., Benedix G., Ehlmann A., Mayeda T. and Clayton R. (1994) Low-FeO ordinary chondrites: a nebular origin and new chondrite parent body. *Lunar Planet. Sci. XXV*. Lunar Planet. Inst., Houston. #865 (abstr).

Miller M. F. (2002) Isotopic fractionation and the quantification of ^{17}O anomalies in the oxygen three-isotope system: an appraisal and geochemical significance. *Geochim. Cosmochim. Acta* **66**, 1881–1889.

Miller M. F., Franchi I. A., Sexton A. S. and Pillinger C. T. (1999) High precision D^{17}O isotope measurements of oxygen from silicates and other oxides: method and applications. *Rapid Commun. Mass Spectrom.* **13**, 1211–1217.

Mittlefehldt D. W., McCoy T. J., Goodrich C. A. and Kracher A. (1998) Non-chondritic meteorites from asteroidal bodies. *Rev. Mineral.* **36**, 4.1–4.195.

Niemeyer S. (1980) I-Xe and ^{40}Ar-^{39}Ar dating of silicate from Weekeroo Station and Netschaëvo IIE iron meteorites. *Geochim. Cosmochim. Acta* **44**(1), 33–44.

Olsen E. and Jarosewich E. (1971) Chondrules – First occurrence in an iron meteorite. *Science* **174**, 583–585.

Olsen E., Davis A., Clarke R. S., Schultz L., Weber H. W., Clayton R., Mayeda T., Jarosewich E., Sylvester P., Grossman L., Wang M. S., Lipschutz M. E., Steele I. M. and Schwade J. (1994) Waston – A new link in the IIE iron chain. *Meteoritics* **29**, 200–213.

Onuma N., Clayton R. N. and Mayeda T. K. (1972) Oxygen isotope cosmothermometer. *Geochim. Cosmochim. Acta* **36**, 169–188.

Osadchii E. G., Baryshnikova G. V. and Novikov G. V. (1982) The Elga meteorite-Silicate inclusions and shock metamorphism. *Proc. Lunar Planet. Sci.* **12B**, 1049–1068.

Prinz M., Nehru C. E., Delaney J. S., Weisberg, M., & Olsen E. (1983) Globular silicate inclusions in IIE irons and Sombrerete: Highly fractionated minimum melts. *Lunar Planet. Sci. XIV*. Lunar Planet. Inst., Houston, pp. 618-619 (abstr.).

Ray D., Ghosh S. and Murty S. V. S. (2014) Shock-thermal history of Kavarpura (IVA) Iron: evidences from microtextures and nickel profiling. *Meteorit. Planet. Sci.* **49**(Suppl.) (#5157 (abst.)).

Rubin E. A. (2005) Relationships among intrinsic properties of ordinary chondrites: oxidation state, bulk chemistry, oxygen-isotopic composition, petrologic type, and chondrule size. *Geochim. Cosmochim. Acta*, 4907–4918.

Russell S. S., McCoy T. J., Jarosewich E. and Ash R. D. (1998) The Burnwell, Kentucky, low iron oxide chondrite fall: description, classification and origin. *Meteorit. Planet. Sci.* **33**, 853–856.

Ruzicka A. (2014) Silicate-bearing iron meteorites and their implications for the evolution of asteroidal parent bodies. *Chem. Erde* **74**, 3–48.

Ruzicka A. and Hutson M. (2010) Comparative petrology of silicates in the Udei Station (IAB) and Miles (IIE) iron meteorites: implications for the origin of silicate-bearing irons. *Geochim. Cosmochim. Acta* **74**, 394–433.

Ruzicka A., Fowler G. W., Snyder G. A., Prinz M., Papike J. J. and Taylor L. A. (1999) Petrogenesis of silicate inclusions in the Weekeroo Station IIE iron meteorite: differentiation, remelting,

and dynamic mixing. *Geochim. Cosmochim. Acta* **63**, 2123–2143.

Sanz H. G., Burnett D. S. and Wasserburg G. J. (1970) A precise $^{87}Rb/^{87}Sr$ age and initial $^{87}Sr/^{86}Sr$ for the Colomera iron meteorite. *Geochim. Cosmochim. Acta* **34**, 1227–1239.

Scherstein A., Elliott T., Hawkesworth C., Russell S. and Masarik J. (2006) Hf-W evidence for rapid differentiation of iron meteorite parent bodies. *Earth Planet. Sci. Lett.* **241**, 530–542.

Schrader D. L., Lauretta D. S., Connolly H. C., Goreva Y. S., Hill D. H., Domanik K. J., Berger E. L., Yang H. and Downs R. T. (2010) Sulfide-rich metallic impact melts from chondritic parent bodies. *Meteorit. Planet. Sci.* **45**, 743–758.

Schulz T., Upadhyay D., Münker C. and Mezger K. (2012) Formation and exposure history of non-magmatic iron meteorites and winonaites: clues from Sm and W isotopes. *Geochim. Cosmochim. Acta* **85**, 200–212.

Scott E. R. D. and Wasson J. T. (1976) Chemical classification of iron meteorites. VIII – Groups IC, IIE, IIIF and 97 other irons. *Geochim. Cosmochim. Acta* **40**, 103–115.

Scott E. R. D., Krot T. V., Goldstein J. T. and Wakita S. (2014) Thermal and impact history of the H chondrite parent asteroid during metamorphism: constraints from metallic Fe–Ni. *Geochim. Cosmochim. Acta* **136**, 13–37.

Snyder G. A., Lee D.-C., Ruzicka A. M., Prinz M., Taylor L. A. and Halliday A. N. (2001) Hf-W, Sm-Nd, and Rb-Sr isotopic evidence of late impact fractionation and mixing of silicates on iron meteorite parent bodies. *Earth Planet. Sci. Lett.* **186**, 311–324.

Takeda H., Hsu W. B. and Huss G. R. (2003) Mineralogy of silicate inclusions of the Colomera IIE iron and crystallization of Cr-diopside and alkali feldspar from a partial melt. *Geochim. Cosmochim. Acta* **67**, 2269–2287.

Teplyakova S., Humayun M., Lorenz C. and Ivanova M. (2012) A common parent for IIE iron meteorite and H chondrites. *Lunar Planet. Sci. XLIII.* Lunar Planet. Inst., Houston #1130 (abstr).

Terribilini D., Eugster O., Herzog G. F. and Schnabel C. (2000) Evidence for common break-up events of the acapulcoites/lodranites and chondrites. *Meteorit. Planet. Sci.* **35**, 1043–1050.

Tomkins A. G., Weinberg R. F., Schaefer B. F. and Langendam A. (2013) Disequilibrium melting and melt migration driven by impacts: implications for rapid planetesimal core formation. *Geochim. Cosmochim. Acta* **100**, 41–59.

Troiano J., Rumble D., Rivers M. L. and Friedrich J. M. (2011) Compositions of three low-FeO ordinary chondrites: implications of a common origin with the H chondrites. *Geochim. Cosmochim. Acta* **75**, 6511–6519.

Valley J. W., Kitchen N., Kohn M. J., Niendorf C. R. and Spicuzza M. J. (1995) UWG-2, a garnet standard for oxygen isotope ratios: strategies for high precision and accuracy with laser heating. *Geochim. Cosmochim. Acta* **59**, 5223–5231.

Van Roosbroek N., Debaille V., Pittarello L., Goderis S., Humayun M., Hecht L., Jourdan F., Spicuzza M. J., Vanhaecke F. and Claeys Ph. (2015) The formation of IIE iron meteorites investigated by the chondrule-bearing Mont Dieu meteorite. *Meteorit. Planet. Sci.* **50**, 1173–1196.

Vernazza P., Zanda B., Binzel R. P., Hiroi T., DeMeo F. E., Birlan M., Hewins R., Ricci L., Barge D. and Lockhart M. (2014) Multiple and fast: the accretion of ordinary chondrite parent bodies. *Astrophys. J.* **791**, 120.

Wasserburg G. J., Sanz H. G. and Bence A. E. (1968) Potassium-feldspar phenocrysts in the surface of Colomera, an iron meteorite. *Science* **161**, 684–687.

Wasson J. T. and Kallemeyn G. W. (2002) The IAB iron-meteorite complex: a group, five subgroups, numerous grouplets, closely related, mainly formed by crystal segregation in rapidly cooling melts. *Geochim. Cosmochim. Acta* **66**, 2445–2473.

Wasson J. T. and Richardson J. W. (2001) Fractionation trends among IVA iron meteorites: contrasts with IIIAB trends. *Geochim. Cosmochim. Acta* **65**, 951–970.

Wasson J. T. and Wang J. M. (1986) A nonmagmatic origin of group IIE iron meteorites. *Geochim. Cosmochim. Acta* **50**, 725–732.

Wasson J. T. and Scott E. R. D. (2011) Group IIE iron meteorites: Metal composition, formation, relationship to ordinary chondrites. *Lunar Planet. Sci. XLII.* Lunar Planet. Inst., Houston # 2813 (abstr.).

Yamaguchi A., Kimura M., Barrat J-A. and Greenwood R. C. (2015) Petrology, bulk chemical and oxygen isotopic composition of a low-FeO ordinary chondrite, Yamato 982717. *Lunar Planet. Sci. 46*. Lunar Planet. Inst., Houston #1679 (abstr.).

Associate editor: Dimitri A. Papanastassiou